J. Earth Syst. Sci. (2020)129 90
https://doi.org/10.1007/s12040-020-1360-x

Delineation of shallow structures in Madawara igneous complex, Bundelkhand Craton, India using gravity–magnetic data: Implication to tectonic evolution and mineralization

Animesh Mandal*, Athul Chandroth, Aurobindo Kumar Basantaray and Utsav Mishra

Department of Earth Sciences, Indian Institute of Technology Kanpur, Kanpur 208 016, India.
**Corresponding author. e-mail: animeshm@iitk.ac.in*

MS received 16 August 2019; revised 1 November 2019; accepted 27 December 2019

An integrated gravity–magnetic study has been carried out over Madawara Igneous Complex (MIC) in southern part of Bundelkhand Craton with an aim to decipher shallow crustal configuration and mineralized zones, thereby to improve the understanding of tectonic evolution of the region. Derived gravity and magnetic anomaly maps show good correlation with known geology and have delineated continuity of mafic–ultramafic intrusive bodies in EW direction. Radially averaged power spectrum (2D) and solutions derived from 3D Euler deconvolution have revealed average basement depths for gravity sources as ∼0.3, 1.2 and 3.2 km, whereas for magnetic sources as ∼0.3 and 1.2 km. From this study, these interfaces could be attributed to sedimentary origin for shallowest layer, mafic–ultramafic intrusive for intermediate layer and changes within the granite–gneissic basement for deeper solutions. Two-dimensional inverse modelling of residual gravity anomaly has delineated intrusion of highly dense mafic–ultramafic rocks from deeper part within the granite gneissic complex. Deeper basement from gravity and shallower from magnetic data indicate presence of two-stage magmatism within a subduction setting where the second magmatic emplacement probably occurred with a magma that comprises high magnetic material. High gravity and magnetic anomalies are observed over the mafic and ultramafic rock samples which are already identified (based on previous geochemical studies) as prospective zones for Cr, Ni and PGE mineralization. Thus, it can be inferred from this study that the mafic–ultramafic intrusive bodies are favourable targets for Cr–Ni–PGE mineralisation which may be obtained between a depth range of around 300 m to 3 km. Thus, the study enhances the scope for further integrated geophysical investigation over the identified prospective zones as well as provides important clues on magmatic evolution of the region.

Keywords. Bundelkhand Craton; Madawara igneous complex (MIC); mafic–ultramafic; gravity–magnetic; inverse model; mineralization.

1. Introduction

Formation of igneous complexes are generally associated with magma chamber processes in varied tectonic environment. As a result, their study can provide significant information related to the evolutional history of a region (Polat *et al.* 2011; Su *et al.* 2011; Cai *et al.* 2012; Yellappa *et al.* 2014). Mafic–ultramafic intrusions of such igneous complexes also host variety of valuable ore deposits,

Published online: 11 March 2020

e.g., metallic deposits (Ma *et al.* 2016) especially, the Cu–Ni–Cr and Platinum Group of Minerals (PGM) (Ernst 2007). Hence, detailed subsurface understanding of such igneous complexes and related mafic–ultramafic rocks is essential in accessing the evolutionary history and prospectivity of ore deposits of a region.

Madawara igneous complex (MIC) is a series of EW trending isolated out crops of lensiodal mafic–ultramafic intrusive rocks in the southern part of Bundelkhand Craton (figure 1a, b) (Satyanarayanan *et al.* 2010; Singh *et al.* 2010a, b). These rocks are mainly distributed over a linear region around Madawara village (Singh *et al.* 2010a, b, 2011; Mohanty *et al.* 2018). Over the last few decades, several studies have reported occurrences of Platinum Groups of Elements (PGE) within this ultramafic complex through petrographic and geochemical data analysis (Basu 1986; Farooqui and Singh 2006; Pati *et al.* 2007; Singh *et al.* 2010a, b, 2011; Balaram *et al.* 2013; Satyanarayanan *et al.* 2015). These workers have reported occurrence of platinum group minerals (PGM) and gold mineralization in association with chromite and sulfide bearing ultramafic rocks from some discrete places (e.g., Madawara, Ikauna, and Pindar villages) of MIC. Very recently, an attempt has also been made to understand the petrogenesis and tectonic setting of MIC, thereby its evolutionary history (Mohanty *et al.* 2018; Ramiz *et al.* 2018). However, most of these existing interpretations are based on surface exposure without having sufficient knowledge about the subsurface configurations and physical properties variations. Further, at many places the rock bodies/structures are masked by sedimentary strata and thus, making it very difficult to infer the vertical and lateral continuity of the intrusive rocks or structures. Therefore, an integrated geophysical study is urgently needed in the study area to delineate the subsurface continuity of the exposed mafic–ultramafic bands and associated mineralization zones.

The petro-physical properties of ultramafic rocks mainly depend on the degree of serpentinization, physical and mechanical conditions under which they are formed. The ultramafics of MIC are nearly unmetamorphosed, less deformed but highly serpentinized (Farooqui and Singh 2006; Singh *et al.* 2011). They mostly comprised of dunite, peridotite, hornblende-rich peridotite, pyroxenite, olivine pyroxenite, gabbro and diorite along with several PGE elements and metallic minerals (Farooqui and Singh 2006, 2010; Satyanarayanan *et al.* 2010, 2015; Balaram *et al.* 2013). Accordingly, the reported platinum group of minerals and other metallic minerals are mostly associated with chromite as well as sulphide bearing ultramafic rocks within granitic surroundings. As a result, the target mafic–ultramafic intrusive rocks as well as mineralization zones are expected to have high density, and magnetic susceptibility contrast with respect to the host Bundelkhand gneissic complex (BnGC). Thus, an integrated geophysical study consisting of gravity and magnetic surveys has been carried out over the MIC within the southern part of Bundelkhand gneissic complex (BnGC) in Lalitpur district of Uttar Pradesh (figure 1a, b). The objectives of this study are: (1) to establish the subsurface continuity of mafic–ultramafic intrusive bodies within the MIC belt, (2) to delineate the prospective mineralization zones and related shallow structural features of the region and (3) to throw some light towards understanding the tectonic evolution of the region. The integrated interpretation of gravity–magnetic results and the existing geological information in the region has provided a more complete picture on the tectonic evolution as well as prospective mineralization zones of the region with an increased confidence.

2. Geology

2.1 *Regional geology*

Indian shield is divided into five major cratonic units, namely Dharwar, Bastar, Singhbhum, Bundelkhand, and Aravalli (Mondal *et al.* 2002; Meert and Pandit 2015). The northern part of the Indian shield comprises of Bundelkhand and Aravalli cratons which are separated from southern cratonic units by Central Indian Tectonic Zone (CITZ) (figure 1a, inset). Bundelkhand Craton is one of the Archean cratons situated in the north central part of Indian Shield and exposed over $\sim$26,000 km^2 area in semi-circular shape (figure 1a) (Basu 1986; Remiz *et al.* 2018). It is bounded by the Son–Narmada Lineament in the south, the Great Boundary Fault in the west, and overlain by the Indo-Gangetic alluvium in the north. It is mostly overlain by Vindhyan supergroup of rocks from east, west, and south (figure 1a). The craton comprises of Archean Bundelkhand gneissic complex (BnGC), volcano-sedimentary units, Madawara igneous complex

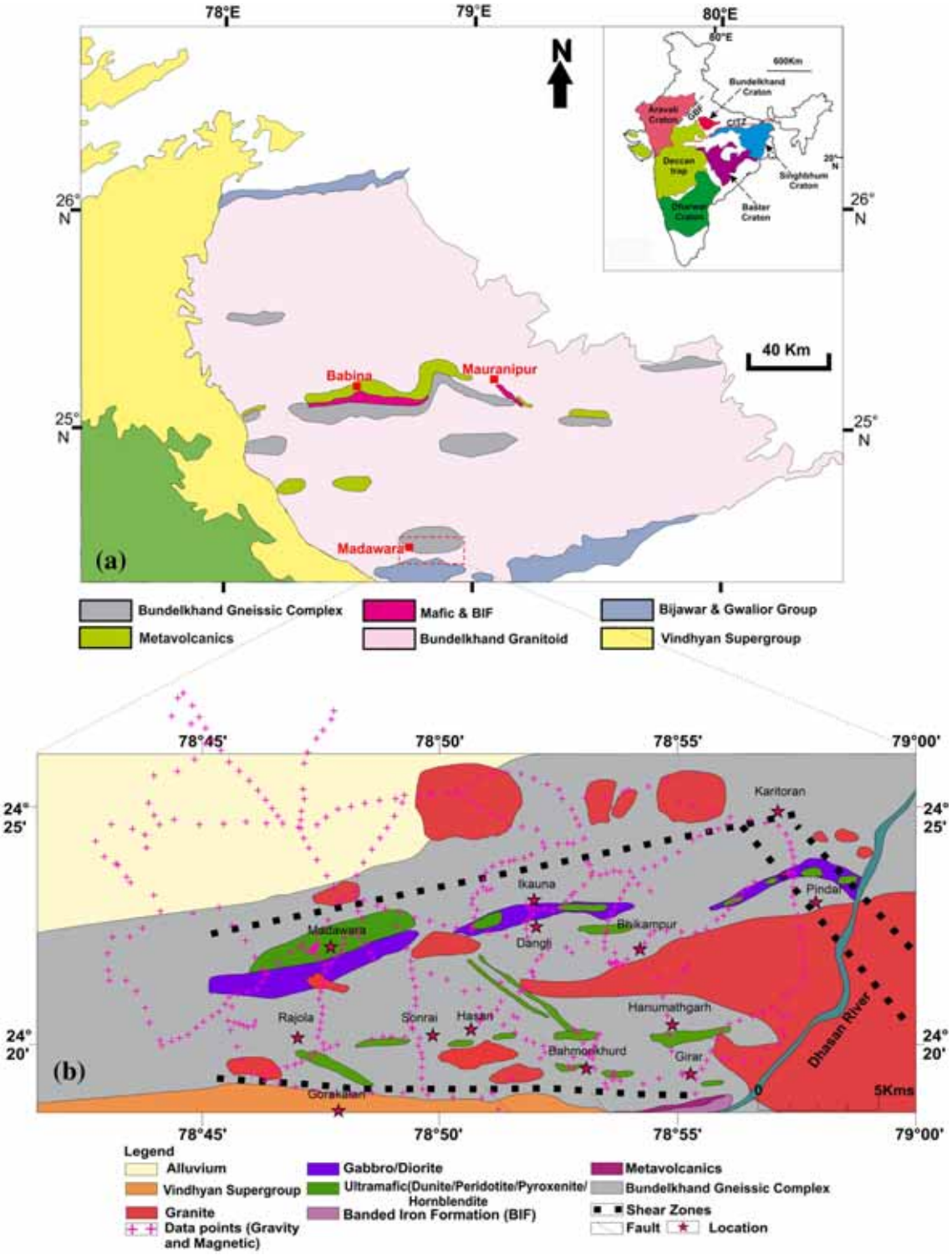

Figure 1. (**a**) Regional geological map of Bundelkhand and its surrounding with geological and tectonic set-up of India in inset (after Mohanty *et al.* 2018). The present study area is marked as dotted rectangle at Madawara, (**b**) local geology map of Madawara Igneous Complex (MIC) and its surroundings with geophysical survey locations marked as '+' (modified after Singh *et al.* 2011; and Mohanty *et al.* 2018).

(MIC), Bundelkhand granitoids, quartz reefs and mafic dykes as major litho-units (figure 1a) (Basu 1986, 2007; Pati *et al.* 2007; Ram Mohan *et al.* 2012; Bhattacharya and Singh 2013). Occurrences of mafic and ultramafic rocks in the southern part of Bundelkhand massif have also been reported

from different places (Prakash *et al.* 1975; Basu 1986). The mafic–ultramafic rocks associated with gabbro and diorite in the granite–gneissic terrain around Madawara is known as Madawara ultramafics complex or Madawara Igneous Complex (MIC). Previous geochemical and geological investigations also reported PGE mineralization within these ultramafic rocks (Farooqui and Singh 2006; Singh *et al.* 2010a).

2.2 *Local geology of the study area*

The present study area is located in the southern part of Bundelkhand Craton between latitudes 24°17′–24°28′N and longitudes 78°43′–78°59′E and covers a total area of approximately 600 km^2 (figure 1b). Exposures of E–W trending mafic–ultramafic rocks as scattered lensoidal intrusive are reported around Madawara, Ikauna, Girar and Pindar villages and collectively known as MIC (figure 1b; Satyanarayanan *et al.* 2010; Singh *et al.* 2010a, b). These lenses of mafic–ultramafic rocks are characterized by different dimensions (500–1500 m in length and 50–600 m in width) consisting of dunite, peridotite, pyroxenite, olivine pyroxenite, hornblendite, gabbro, diorite, and distributed over a region of 40 km length and 2–4 km wide (Satyanarayanan *et al.* 2010, 2015; Mohanty *et al.* 2018; Ramiz *et al.* 2018). The largest (∼3 km in width and ∼4–5 km in length) ultramafic body is exposed at Madawara village. This region is also dominated by several NW–SE trending shear faults/fractures and that could be the triggering cause of ultramafic bands (Singh *et al.* 2010a, b). The mafic–ultramafic rocks of MIC are mainly confined between the Madawara–Karitoran shear zone in the north and Sonrai–Girar shear zone in the south (Balaram *et al.* 2013; Satyanarayanan *et al.* 2015; Ramiz *et al.* 2018). These northern and southern contacts between mafic–ultramafic rocks and granite–gneisses of BnGC is sharp, sheared and mylonitized in nature. Detailed geochemical and petographical analyses of these rocks indicated the presence of platinum group of minerals (PGM) and also gold associated with chromite and sulphide bearing ultramafic rocks (Singh *et al.* 2010a, b, 2011; Satyanarayanan *et al.* 2010, 2015; Balaram *et al.* 2013). Recent geochemical studies indicate that the MIC is formed due to subduction-related magmatism in the southern part of Bundelkhand Craton and subsequent rise of asthenospheric mantle (Mohanty *et al.* 2018; Ramiz *et al.* 2018).

3. Methodology

An integrated geophysical study using gravity and magnetic methods was employed in the study area based on the available geological information and expected physical property contrast in the study area. The methodology adopted for each of the cases is outlined in the following sections.

3.1 *Gravity data*

The gravity data were acquired at 467 locations (figure 1b) covering an area of ∼600 km^2 around Madawara area using Scintrex CG-6 gravimeter (with resolution 0.001 mGal). Gravity observation points were established along different approachable roads with a station spacing varying between 200 and 400 m. All the gravity observations were tied to a nearby base station (Gravity base IGSN1971 – Geological Survey of India) established at Ronra, Lalitpur (lat: 78°25′56″N, long: 24°44′14″E, elevation 357.775 m, 978,806.046 mGal) after employing drift correction. The theoretical gravity value at each location was calculated using Geodetic Reference System 1967 (GRS67). Free-air correction term was calculated by the standard free-air gradient of 0.3086 mGal/m (neglecting higher order terms). To compute the Bouguer correction, an average crustal density of 2670 kg/m^3 was assumed. Digital elevation model (DEM) was created from the acquired DGPS data, and was used for topographic correction. The elevation of the study area varied from ∼350 to ∼418 m and corresponding maximum terrain correction value is ∼0.0419 mGal. Thus, all the raw gravity data were subjected to drift (based on repeat reading), free-air, bouguer and terrain corrections to calculate the Bouguer anomaly values at each location. Elevation data and the calculated Bouguer anomaly values are presented as contour maps using minimum curvature gridding technique in Geosoft software (figure 2a and b, respectively).

3.1.1 *Regional residual separation*

Bouguer anomaly comprises of the gravity signatures due to deep seated (regional anomaly) and shallow sources (residual anomaly). Separation of the regional component from the Bouguer anomaly is an important step in gravity data interpretation to delineate the shallow crustal configuration. In this study, an upward

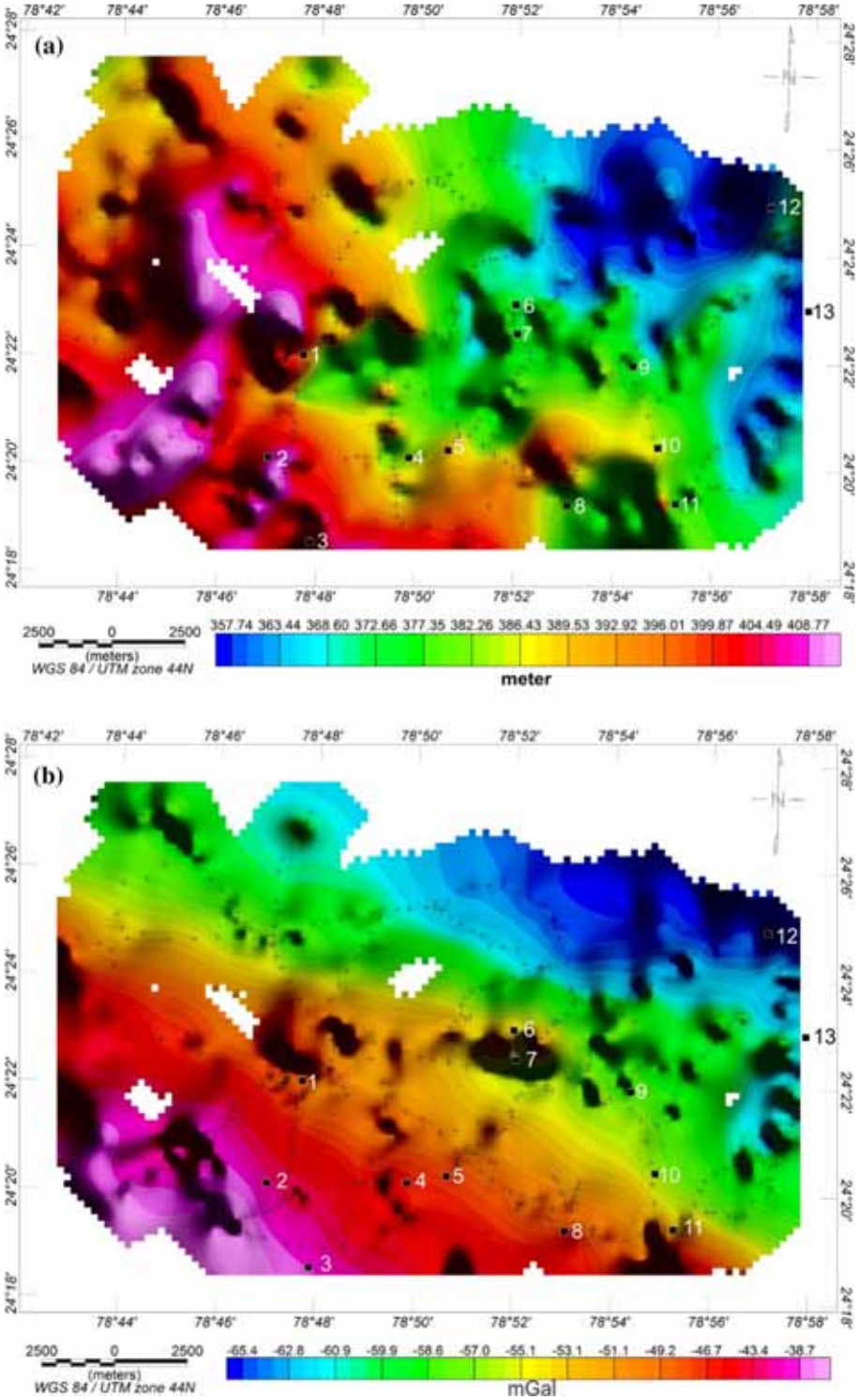

Figure 2. (**a**) Elevation map and (**b**) complete Bouguer anomaly map of the study area. Symbol '+' shows the gravity survey locations. Locations of the major localities/villages are marked with black rectangles as: (1) Madawara, (2) Rajola, (3) Gorakalan, (4) Sonrai, (5) Hasari, (6) Ikauna, (7) Dangli, (8) Bahmorikhurd, (9) Bhikampur, (10) Hanumatgarh, (11) Girar, (12) Karitoran, and (13) Pindar.

continuation filter (Pacino and Introcaso 1987; Blakely 1995) was utilized to obtain the regional gravity effect from the Bouguer anomaly data in Geosoft software. The upward continued map corresponding to 10 km above the geoid was found to decipher the regional trend sufficiently at each grid node of Bouguer anomaly grid (figure 3a). The residual gravity anomaly map (figure 3b) was

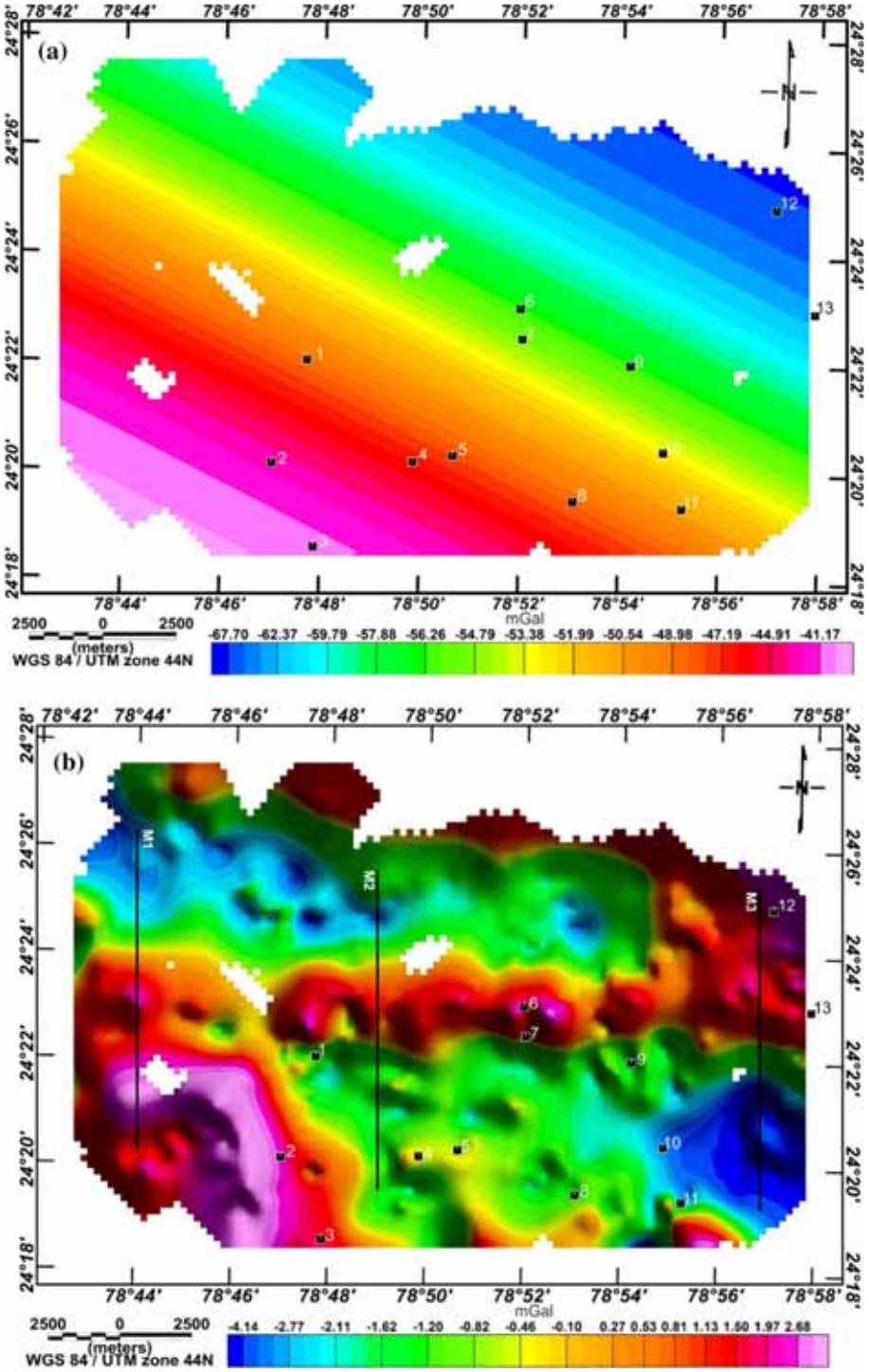

Figure 3. (**a**) Regional and (**b**) residual gravity anomaly maps of the study area. M1, M2, and M3 are three profiles for inverse modelling. Locations of the major localities/villages are marked with black rectangles as: (1) Madawara, (2) Rajola, (3) Gorakalan, (4) Sonrai, (5) Hasari, (6) Ikauna, (7) Dangli, (8) Bahmorikhurd, (9) Bhikampur, (10) Hanumatgarh, (11) Girar, (12) Karitoran and (13) Pindar.

obtained by substracting these regional anomaly values from the Bouguer anomaly map.

The estimated regional anomaly map (figure 3a) has effectively revealed the smoothly varying SW–NE trending high-low gravity anomaly variation of the Bouguer anomaly map. East–west trending high residual gravity anomaly matches with the location of exposed mafic–ultramafic rock bands around Madawara (1), Ikuana (6) and Pindar (13) villages at the central part of the study area (compare figures 1b and 3b). Thus, the separated anomaly maps show good correlation with

the regional trend and exposed surface geology of the study area.

3.2 *Magnetic data*

In the present study, magnetic measurements were carried out at the same 467 gravity observation locations around Madawara area (figure 1b). All the magnetic measurements were carried out using GSM 19T Proton Magnetometer with resolution 0.01 nT. The acquired magnetic data were subjected to diurnal and International Geomagnetic Reference Field (IGRF-2015) corrections to get the total field magnetic anomaly values which are then presented as a contour map using minimum curvature gridding technique in Geosoft software (figure 4a). Unlike gravity anomalies, magnetic anomalies do not appear vertically above the anomalous body and are asymmetric in nature due to dipolar behaviour of the earth's magnetic field away from the poles and equator (Baranov 1957; Roest and Pilkington 1993). These distortions in magnetic anomalies can be eliminated by reduction-to-pole (RTP) transformation using various approaches (Baranov 1957; Spector and Grant 1970; Nabighian 1972; Roy and Aina 1986; Silva 1986). The average inclination and declination of the study area are 37.67° and 0.39°, respectively. In the present study, the total field magnetic anomaly data were reduced to pole by using a Fourier domain filtering technique (Blakely 1995) in Geosoft software (figure 4b) to bring the symmetrical anomaly above the causative source.

3.3 *Depth estimation*

One of the major applications of gravity–magnetic data is to estimate the depth to the top of causative geologic sources and to decipher the basement configuration. In the present case, delineation of the depth and lateral continuity of the igneous intrusive bodies as well as shear zones is an important aspect. Three approaches namely, radially average power spectral analysis, 3D Euler deconvolution and two-dimensional residual gravity modelling have been utilized in this study.

3.3.1 *Radially averaged power spectrum (RAPS) technique*

2D radially averaged power spectrum (RAPS) analysis is one of the most useful and dependable technique to estimate the depth to the top of the gravity–magnetic sources (Naidu 1970; Spector and Grant 1970; Tselentis *et al.* 1988). It relies on the spectral analysis of gravity–magnetic anomaly data in Fourier domain. Applying Fast Fourier Transform (FFT), radially averaged power spectrum of Bouguer gravity anomaly and RTP magnetic anomaly data has been calculated. The natural logarithm of power of respective anomaly has been plotted against wavenumber and corresponding depth estimation plot was generated by finding the slope of the line joining five successive points and dividing by -4π using Geosoft software. 2D RAPS of both the gravity and magnetic data, and the estimated linear slopes are shown in figure 5(a, b), respectively. The average depth to the causative sources is estimated from the linear slopes of these plots.

3.3.2 *Euler deconvolution*

The Euler deconvolution, based on Euler's homogeneity equation (Thompson 1982), is another popular tool to estimate the source depth locations from the observed anomalous potential field data. In the present study, 3D Euler deconvolution technique (Reid *et al.* 1990) has been applied on gridded Bouguer gravity and reduced-to-pole magnetic anomaly data. The locations and depths (x_0, y_0, z_0) of the respective sources are estimated by solving the following 3D Euler's equation:

$$(x-x_0)\frac{\partial f}{\partial x}+(y-y_0)\frac{\partial f}{\partial y}+(z-z_0)\frac{\partial f}{\partial z}=-N(B-f), \quad (1)$$

where f is the observed potential field (gravity or magnetic) at (x, y, z) (coordinates of grid nodes), B is the base level of the field (e.g., the regional value at (x, y, z)) and N is the Euler's structural index (SI) (degree of homogeneity) whose value depends on the geometry of the source bodies. The gradients of the field along three orthogonal axes are calculated using fast Fourier transform (FFT). Assuming the SI, this set of equations are simultaneously solved for source position at each grid point within a sub-grid or window in least square sense using Geosoft software. The size of the window has to be chosen in such a way that it should not include effects of multiple sources but at the same time should cover substantial field variations. The quality of the depth estimation also depends on the choice of SI. Thus, based on the anomaly

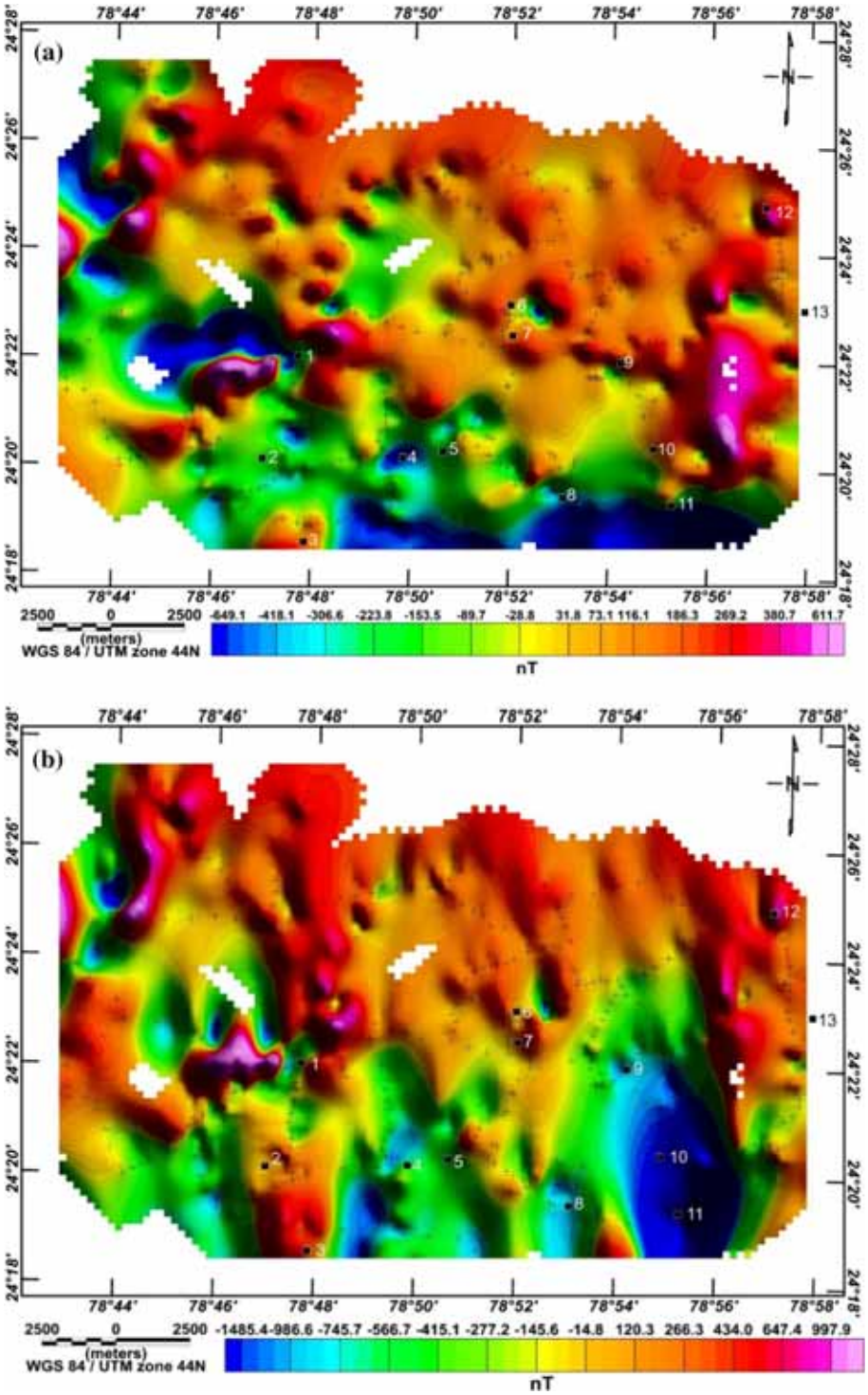

Figure 4. (**a**) Total field magnetic anomaly and (**b**) reduced-to-pole (RTP) total field magnetic anomaly maps; symbol '+' shows the magnetic survey locations. Locations of the major localities/villages are marked with black rectangles as: (1) Madawara, (2) Rajola, (3) Gorakalan, (4) Sonrai, (5) Hasari, (6) Ikauna, (7) Dangli, (8) Bahmorikhurd, (9) Bhikampur, (10) Hanumatgarh, (11) Girar, (12) Karitoran and (13) Pindar.

pattern, the 3D Euler deconvolution technique has been applied in the present study using a window size of 10 grid cells, depth tolerance of 15% and with varying SI in Geosoft software to further confirming the results of RAPS analysis. The Euler's depth solution from Bouguer gravity and RTP magnetic anomaly data are estimated with SI of 0, 1, 2 (for gravity) and 1, 2, 3 (for magnetic), respectively, based on available geological information (figures 6 and 7).

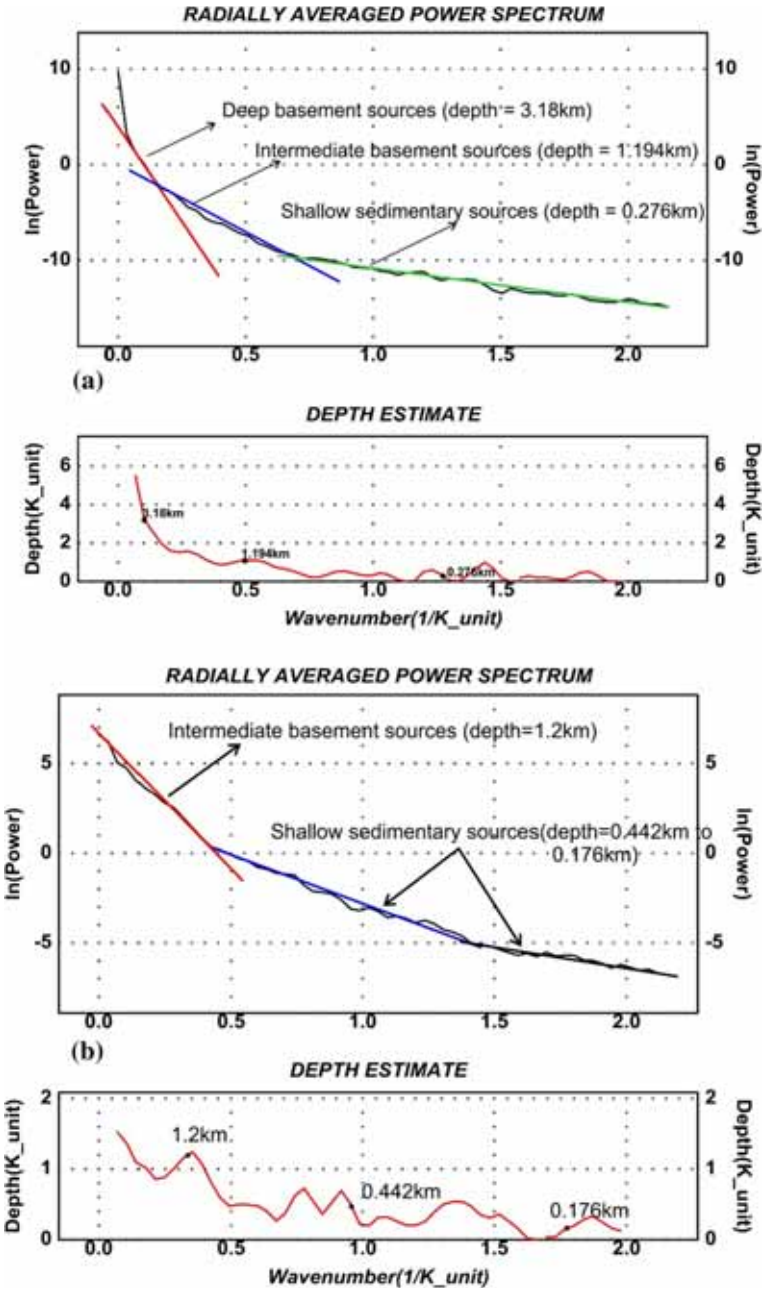

Figure 5. 2D radially averaged power spectrum plot (upper panel) and corresponding depth section (lower panel) plot for (**a**) Bouguer gravity anomaly data and (**b**) RTP total field magnetic anomaly data.

3.3.3 *2D inverse gravity modelling*

The 2D inverse modelling of the residual gravity data along three selected NS profiles are carried out using the modified compact gravity inversion approach as proposed by Srivastava *et al.* (2018). According to this approach, the subsurface is divided into M number of right rectangular blocks whose densities (m_j) are allowed to vary both laterally as well as vertically and their cumulative effect provides the gravity value at certain location (g_i) given by

$$g_i = \sum_{1}^{M} A_{ij} m_j, \tag{2}$$

where $i = 1, 2, \ldots, N$; number of observations.

Elements of the kernel matrix A_{ij} quantifies the contribution of the jth cell of unit density to the ith gravity measurement point and depends on the geometry of the blocks as well as their relationship to the observation points. This modified scheme iteratively solves equation (2) for model parameter m based on weighted least square technique. After kth iteration, the solutions are

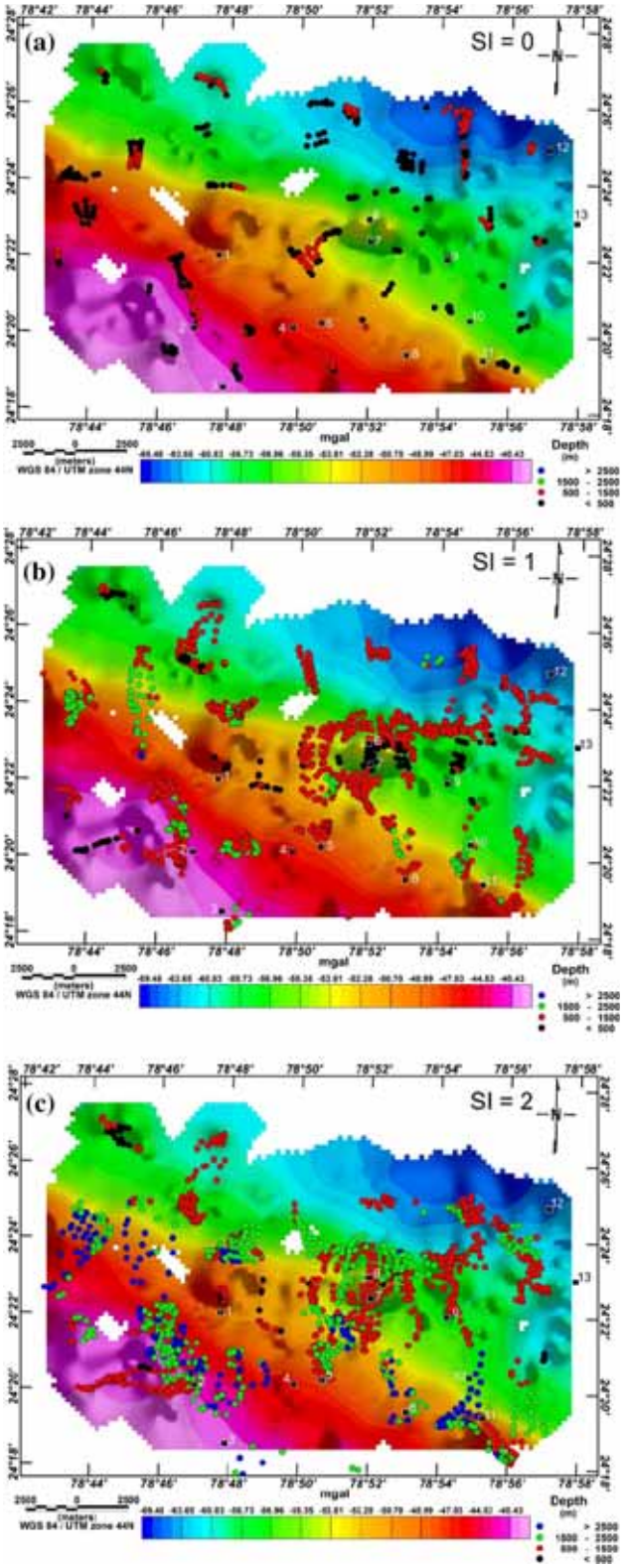

Figure 6. Euler depth solutions of Bouguer gravity data using different structural indices; (**a**) SI = 0, (**b**) SI = 1, (**c**) SI = 2. Source depth is represented by filled circles of different colours.

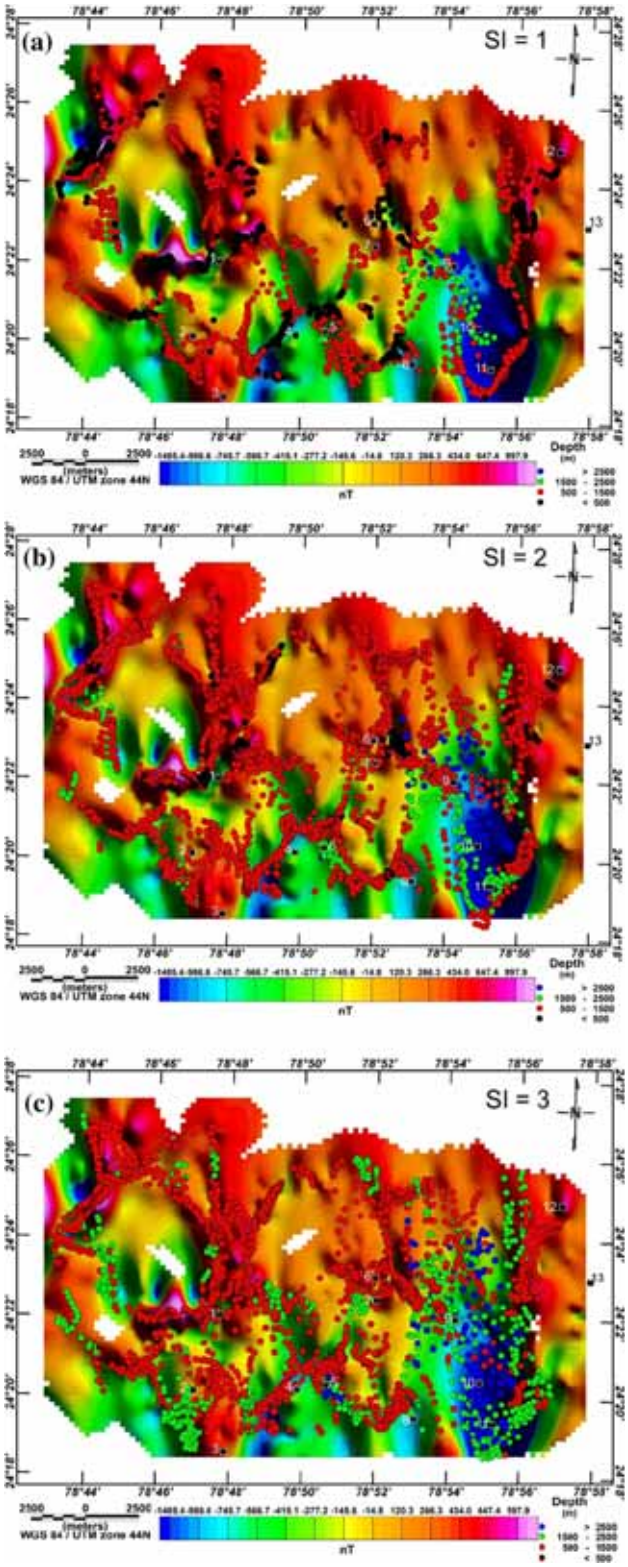

Figure 7. Euler depth solutions of RTP total field magnetic anomaly data using different structural indices; (**a**) SI = 1, (**b**) SI = 2, (**c**) SI = 3. Source depth is represented by filled circles of different colours.

updated using a probabilistic bound as introduced by Srivastava *et al.* (2018) and given as:

$$m^{k+1} = 0.95m^k + W_{m(k)}^{-1} A^T \times \left[A\, W_{m(k)}^{-1} A^T + \varepsilon_0^2\, W_{e(k)}^{-1}\right]^{-1} \left[g_{obs} - Am^k\right], \quad (3)$$

where W_m and W_e are the model and error weighing matrices, respectively, ε_0 is the damping factor (regularization parameter) (Srivastava *et al.* 2018). In the present study, inversion was initialized with a zero-reference model and the damping factor is chosen to be 1.21 based on several trials. Based on the local geological information, the mafic–ultramafic rocks are intruded within granitic-gneissic basement and at places covered with alluvium (figure 1b). Therefore, the density values of the blocks are constrained between a minimum of 2000 kg/m^3 to a maximum of 3070 kg/m^3 (Telford *et al.* 1990) for the inverse modelling.

4. Results

4.1 *Gravity*

The Bouguer anomaly map (figure 2b) shows high to low decreasing trend from southwest to northeast direction. Overall, Bouguer gravity anomaly variation within the study area is ∼29 mGal, with a minimum of −69.48 mGal and maximum of −40.43 mGal. Distinct high gravity anomalies are observed at the central and southwestern parts of the study area. There exists a gradual high to low transition zone along the SW–NE direction of the study area. This indicates the existence of different crustal material and/or structure across NW–SE diagonal.

Upward continued regional gravity anomaly map (figure 3a) has effectively deciphered the SW–NE decreasing trend of the Bouguer anomaly map of the study area. A better correlation with the exposed mafic–ultramafic rocks and shallower features is also observed in the calculated residual anomaly map (figure 3b). It reveals an E–W trending high gravity band from Madawara (1) to Pindar (13) villages at the central part of the study area bounded by relatively low gravity zones towards both northern and southern sides of this band (figure 3b). These exactly correlate with the exposed ultramafic–mafic rocks of E–W trending MIC, situated between the Madawara–Karitoran Shear in the north and the Sonrai–Girar Shear in the south (figures 1b and 3b). High to low gravity transition towards north of Madawara (1), Ikauna (6) and Karitoran (12) villages mark the northern boundary of MIC as Madawara–Karitoran shear. Prominent high gravity patches are also observed at the SW (i.e., southwest of Rajola (2) and Gorakalan (3) villages) and NE (i.e., area between Karitoran (12) and Pindar (13) villages) corners of the study area (figure 3b). Some moderately high discrete gravity anomaly patches are also observed near Sonrai (4), Hasari (5), Bahmorikhurd (8), and Girar (11) villages. A distinct low gravity anomaly circular patch is observed at the SE corner of the study area towards NE of Girar (11) and east of Hanumatgarh (10) villages. Another low gravity zone is observed towards NW part of the study area (figure 3b). Moderate to high gravity transition zone towards the extreme southern part of the residual gravity anomaly map decipher the southern boundary of MIC as Sonrai–Girar Shear (figure 1b and 3b). Thus, all these high gravity anomaly patches may be caused by high density mafic–ultramafic intrusive bodies at shallow crustal depths. This can be further confirmed from the results of magnetic study.

4.2 *Magnetic*

The magnetic total field anomaly map (figure 4a) shows high and low anomaly patches all over the area with a distinct EW high anomaly trend at the central part of the area. Overall, the magnetic total field anomaly values in the study area varies from −649.1 to 611.7 nT. The magnetic anomaly map was further enhanced by applying reduced-to-pole (RTP) transformation in Geosoft software (figure 4b). Magnetic highs as observed near Madawara (1), Rajola (2), Gorakalan (3), Ikauna (6), Dangli (7), Karitoran (12) and Pindar (13) villages reveal good correlation with the exposed outcrops of mafic–ultramafic rocks in the same region (figures 1b and 4b). In general, northern part of the study area shows higher magnetic anomaly values compared to southern part (figure 4a, b). The high magnetic anomaly patches near Madawara (1), Ikauna (6), Dangli (7), and Karitoran (12) villages depict good correlation with exposed ultramafic patches as well as with the EW trending high residual gravity anomaly at the middle part of the study area (figures 1b, 3b, and 4b). Thus, the study depicts the continuation of the exposed ultramafic bands of Madawara (1), Ikauna

(6), Dangli (7), and Karitoran (12) in almost EW direction at the central part of the study area. Similar correlations between high residual gravity and magnetic anomaly are also observed along NS direction around Rajola (2) and Gorakalan (3) villages. Moderate high magnetic anomaly patches near villages Sonrai (4), Hasari (5), and Bahmorikhurd (8) also depict good correlation with moderately high discrete gravity anomaly patches around the same region (figures 3b and 4b). Low magnetic anomaly patch around Girar (11) and Hanumatgarh (10) villages exactly coincide with the lowest gravity anomaly patch of the study area. Such zones with low gravity and magnetic anomalies indicate the presence of granite batholiths in these regions. However, the regions with moderate to high coincident gravity and magnetic anomalies indicate the presence of mafic–ultramafic intrusive bodies.

4.3 *Depth estimation*

Spectral analysis of gravity/magnetic anomaly indicates an ensemble average depth to the different sources of anomalies, thereby provide depth information of subsurface layers or basement configuration (Naidu 1970; Spector and Grant 1970). In the present study, the 2D radially average power spectra of the Bouguer gravity anomaly (figure 5a) reveal three main linear segments, namely, (i) a low wavenumber end that is caused by deeper discontinuities (e.g., deeper basement boundaries), (ii) middle wavenumber range, with an undulating character, may be caused by shallower sources (due to intrusions or intermediate basement features), and (iii) a high wavenumber segment which may be noise or near surface features (e.g., density contrasts within the top sedimentary layers). The calculated average depth of the causative sources from Bouguer gravity anomaly data are 3.18, 1.19 and 0.27 km for deep basement, intermediate basement and shallow sources, respectively (figure 5a). However, power spectrum of RTP total field magnetic anomaly reveals two layer configuration with their average depths of 1.2 km and 0.44–0.18 km (avg. 0.31 km), respectively (figure 5b).

Calculated Euler solutions from Bouguer anomaly and RTP magnetic anomaly data are plotted as coloured circles over the corresponding anomaly contours in figures 6(a–c) and 7(a–c), respectively. In the present study, structural index corresponding to thin sheet edge/sill/dyke/steep contact, pipe/vertical pole and spherical sources, i.e., 0, 1, 2 (for gravity data) and 1, 2, 3 (for magnetic data) are used to achieve the best possible solution (Reid and Thurston 2014). The Euler solution for SI = 0 (for gravity data) reveals the depth of the lateral boundaries or contact zones mainly in the range of <500 m (figure 6a). Euler depth solutions for SI = 1 are mostly concentrated in the central part with depth ranges between 500 and 1500 m with few solutions in depth range < 500 and 1500–2500 m. A thick clustering in the Euler solutions is achieved with SI = 2 indicating causative sources are spherical in nature. Depth of these solutions ranges mostly between 500–1500 and 1500–2500 m with some having depth > 2500 m (figure 6c). The Euler depth solution for SI = 1.0 for magnetic data demarcates the lateral boundary with depth in all ranges (figure 7a); however, mostly clustered in the depth range 500–1500 m with few <500 m (figure 7a). For SI = 2.0, the Euler depth solution gives a good clustering in the depth range 500–1500 m with some solutions in depth range 1500–2500 m and >2500 m (figure 7b). For SI = 3, more clustering in Euler solutions is obtained in the depth range 500–1500 m with some within 1500–2500 m due to the spherical type body (figure 7c). In all the three cases, few deeper solutions with depth >2500 m are obtained for magnetic data but they are related to lowest magnetic anomaly zone, thus, may not be due to subsurface magnetic material. Thus, the magnetic sources are mainly concentrated within shallow (<500 m) or intermediate depth (500–1500) which is in accordance with the results of RAPS.

In the present study, subsurface density modelling has also been carried out using the modified compact inversion approach (Srivastava *et al.* 2018) for residual gravity anomaly along three profiles M1, M2 and M3 (aligned in NS direction from west to east, figure 3b) to further confirm the subsurface configuration. Based on the information of RAPS and Euler solution, the inversion was carried out using three layers as 0–500, 500–1500 and 1500–4000 m. These layers have been gridded with square blocks of 25 × 25, 50 × 50 and 150 × 150 m, respectively. The constraints on the density values are obtained from the known surface geology. Most of the study area was covered by granite gneiss with top soil/alluvium with occasional intrusive mafic/ultramafic band. Thus, a density contrast from 400 to –670 kg/m^3

was applied with respect to the basement density of 2670 kg/m^3 to carry out inverse modelling. A zero-reference model is utilized for initialization and the damping factor is chosen to be 1.21 based on several trials. The best fitted models are obtained by minimizing the density variations of last successive iteration and are shown in figure 8(a–c). The rms misfits for the best fitted models along profiles M1, M2 and M3 are 0.0241, 0.0177 and 0.0218, respectively. The low-density zone around 2000–3500, 2000 and 1000 m locations of profile M1, M2 and M3, respectively, indicates the traces of Madawara–Karitoran Shear zone (figures 1b, 3b and 8a–c). The width and depth extension of this low-density shear zone is varying from 500 and 1500 m in the western side to 500 and 1000 m in the eastern part, respectively (figure 8a–c). Another low-density zone nearly at 7000, 6750 and 6000–8000 m locations of profiles M1, M2 and M3, respectively, indicates the traces of Sonrai–Girar Shear zone (figures 1b, 3b and 8a–c). The width and depth of the shear zone is increasing towards eastern side (figure 8a–c). The high-density discontinuous lensoidal pods with varying length and depth extension are observed in the modelled sections of the three profiles below the observed EW trending high residual gravity anomaly zone (figures 3b and 8a–c). Thus, the high-density pods around 5500–6000, 4000–5000, and 4000–4500 m locations along the density section of M1, M2 and M3, respectively, reveals the EW continuation of the target mafic–ultramafic rocks of MIC. Depth-wise, these highest density pods are extended between nearly 300 m to 2 km along M1, 250 m to 3 km along M2, and 500 m to 1.5 km along M3. Thus, it is extending up to a maximum depth of ∼3 km near Madawara village and may be going beyond the maximum modelled depth of 4 km at some places suggesting existence of their deeper connectivity.

5. Discussion

Geological map of MIC (figure 1b) shows outcrops of mafic–ultramafic rocks mostly aligned in EW direction (with few in NW–SE direction) as discrete lensoidal pods of different dimensions as intrusive bodies within Bundelkhand gneissic complex. As a result, these mafic and ultramafic rocks could be responsible for strong gravity and magnetic anomalies. Thus, the present gravity–magnetic data has helped to unravel the

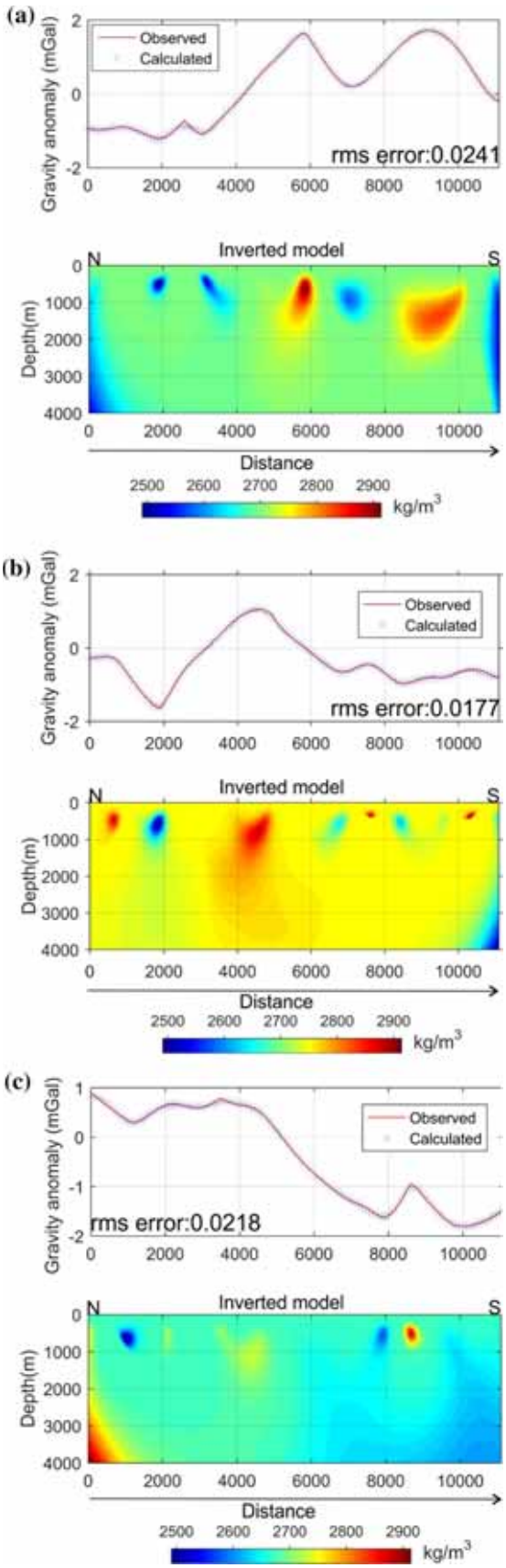

Figure 8. Two-dimensional inverse modelling of residual gravity anomaly along (**a**) profile M1, (**b**) profile M2, and (**c**) profile M3.

subsurface structures and geotectonic evolution of the MIC.

Coincidence of high gravity and magnetic anomaly at the central part of the study area between Madawara (1) and Karitoran (12) villages strongly indicates the subsurface continuation of mafic–ultramafic intrusive rocks within gneissic complex (figures 1b, 3b and 4b). Towards further west of Madawara village, this mafic–ultramafic band may be continuing along SW and SSW direction (between Rajola (2) and Gorakalan (3) villages; figures 1b, 3b and 4b). Similar correlation between gravity–magnetic anomalies also indicate the presence of mafic–ultramafic rocks between Karitoran (12) and Pindar (13) villages (figures 3b and 4b). Lowest gravity and magnetic anomaly towards SE corner of the study area around Girar (11) and Hanumatgarh (10) villages may be attributed to Granite batholiths and sedimentary cover (figures 1b, 3b and 4b). Bundhelkhand gneissic complex in the south-central part of the study area is revealed by moderate gravity–magnetic anomaly. Lowest gravity and high-low magnetic patches in the NW part of the study area can be attributed to the presence of thick alluvium in the shallow subsurafce (figures 1b, 3b, and 4b). Thus, coincidence of moderate to high gravity and high magnetic anomaly suggest existence of mafic–ultramafic rocks in the subsurface.

Distinct gravity anomaly gradients towards north (high to low) and south (low to high, extreme southern part) of the central high anomaly zone (figure 3b) indicate the presence of Madawara–Karitoran and Sonrai–Girar Shear zones, respectively. These shear zones may be produced due to the shear stress exterted by the mafic intrusion, which resulted in crustal rock deformation and metamorphism in the adjacent northern and southern parts of the area, resulting in less dense granitic rock bodies identified as Bundhelkhand granitoid and Bundhelkhand gneissic complex. Trend of the gravity anomaly indicates that the Madawara–Karitoran and Sonrai–Girar shear zones may be extending outside the study area towards west and east direction, but truncated near NE and SW part of the study area, respectively (figures 1b and 3b). Trend of these shear zones and mafic–ultramafic rocks at central part of the study area is mostly in E–W direction and oriented in SW–NE direction towards the edge of the study area. This trend matches well with the general trend of Central Indian Tectonic Zone (CITZ) which formed in a subduction environment by the collision of a southern protocontinent and a northern protocontinent (Naganjaneyulu and Santosh 2010; Bhowmik *et al.* 2012). This structural similarity as well as results from recent geochemical studies (Mohanty *et al.* 2018; Ramiz *et al.* 2018) suggest that the MIC also formed by same tectonic processes in a subduction setting.

Radially average power spectra analysis of gravity anomalies revealed two distinct shallow interfaces at depths $\sim$1.2 and $\sim$0.3 km with deepest interface at $\sim$3.2 km. However, the power spectrum analysis of magnetic data reveals two layers at $\sim$1.2 and $\sim$0.3 km depths. There exists a consistency in the shallow interface at $\sim$1.2 km depth as obtained from power spectrum analysis of both gravity and magnetic data. Based on the local geology and magnetic signature, it can be inferred that the shallowest layer associated with sedimentary sources and intermediate basement mostly consists of high magnetic mafic/ultramafic intrusive rocks. Below this intrusive unit, there exists a high density basement layer with average depth to the top of the layer is $\sim$3.2 km. These results are consistent with the findings of 3D Euler deconvolution and later suggest the sources as dyke and spherical in shape which also agrees with existing geological knowledge of the region. The two different basement depths as obtained from gravity (deeper) and magnetic (shallower) data may indicate two different products from same location at different times (i.e., two-stage magmatism). A second magmatic emplacement with a magma of high magnetic materials might have resulted into such shallow magnetic basement. In other words, two different magma sources may have caused the formation of these mafic–ultramafic assemblages of MIC. Most feasible model for such magma emplacement is the continental arc setting of a subduction set-up as proposed by Ramiz *et al.* (2018), in which an oceanic crust from southern part of the study area is subducting under the continental crust of the northern side. Therefore, the present findings provide independent support for the subduction model proposed by Ramiz *et al.* (2018).

2D inverse modelling of residual gravity anomaly based on the quantitative information from above two appraoches as well as available geological knowledge has helped to understand the subsurface configuration of the study area. Highest density patches ($\sim$2800–2900 kg/m^3) near to central part of the NS profiles M1 (western side of study area) and M2 (central part of study area) deciphered

presence of mafic–ultramafic target from ∼250–300 m depth and extending up to a depth of ∼2 km in M1 and ∼3 km in M2 (figure 8a, b). Along the NS profile M3 (east of M2), high surface RTP magnetic anomaly correlates with high residual gravity anomaly (figures 3b and 4b). Further, the modelled section revealed the presence of comparatively high density (∼2750 kg/m^3) bodies but not as high as that of along M1 and M2 (figure 8c). Thus, subsurface models also indicate the presence of mafic–ultramafic rocks with relatively low density material (compared to M1 and M2). Such reduction in density may be caused by serpentization of mafic–ultramafic rocks (Toft *et al.* 1990; Clark 1997). Models also reveal that these high density bodies of MIC are mostly dipping towards north. This also indirectly provide support for the subduction model as discussed above.

Detailed petrological and geochemical analysis of mafic and ultramafic rock samples carried out for last two-three decades from Madawara, Ikauna, and Pindar villages of MIC have already identified as prospective zones for Cr, Ni and PGE mineralization (Farooqui and Singh 2006; Satyanarayanan *et al.* 2010; Singh *et al.* 2010a, b; Balaram *et al.* 2013). However, detailed exploration activities have not been yet taken up in this region. For the first time, a geophysical investigation has been carried out in MIC to delineate the subsurface configuration of the target mafic–ultramafic exposures. In the present study, very good correlation between high to moderate gravity and high magnetic anomalies are observed not only in and around Madawara (1), Ikauna (6), and Pindar (13) villages but also around few more new villages, viz., Rajola (2), Gorakalan (3), Karitoran (12), Sonrai (4), and Hasari (5) (figures 1b, 3b and 4b). Thus, based on geological and geochemical knowledge and correlation of gravity–magnetic signatures, it can be inferred that there exist mafic–ultramafic rocks in subsurface of above-mentioned villages and they can also serve as new prospective zones for Cr–Ni–PGE mineralization in this area. Present geophysical study has deciphered the lateral continuation of mafic–ultramafic band from Madawara to Pindar villages as well as residual gravity modelling has revealed the depth and width of these target zones. Thus, it can be concluded that these mafic–ultramafic intrusive bodies are the favourable targets for Cr–Ni–PGE mineralization within the MIC which may be obtained at a depth range of ∼300 m to 3 km.

6. Conclusions

In the present work, detailed gravity–magnetic study has been performed in conjunction with known geological and geocheminal knowledge of Madawara Igneous Complex (MIC) in the southern part of Bundelkhand craton, India. Residual gravity and RTP magnetic anomalies have effectively deciphered the subsurface continuity of the mafic–ultramafic intrusive body between Madawara and Karitoran-Pindar villages in EW direction. Two-dimensional inverse models of the residual gravity anomaly data were constructed with the depth constraint from power spectrum analysis and Euler solutions. These models suggest that the causative bodies from deeper part of the earth may be intruded in the granite gneissic complex at the central portion of the study area. Maximum depth extension of these target mafic–ultramafic bodies is delineated as ∼3 km. Two different basement depths, as obtained from gravity (deeper) and magnetic (shallower) data, indicate two different products from same location at different times and probably second emplacement occurred with a magma of high magnetic materials. Basement configuration, dipping of high-density bodies, and similarity in the trend of the local shear zones with CITZ indicate that MIC was formed in a subduction setting with two different magma sources at two different times (i.e., two stage magmatism). However, to infer further details on tectonic configuration and evolution of this region more confidently, the present study needs to be integrated with regional scale gravity–magnetic study along with development of a full lithospheric model.

Correlation between high gravity–magnetic anomalies with previously identified high concentration of Cr–Ni–PGE in the mafic–ultramafic samples from Madawara, Ikauna, and Pindar villages has established probable geophysical signature for PGE mineralization in MIC. This has led to delineation of new prospective PGE mineralization zones in MIC belt. 2D inverse modelling of residual gravity anomaly has effectively delineated the lateral and vertical continuation of these target zones. This information will be useful for mineral prospectors. It can be concluded that the mafic–ultramafic intrusive bodies with high-gravity–magnetic anomalies are the favourable targets for Cr–Ni–PGE mineralization within the MIC which may be obtained between a depth range of around 300 m to 3 km. The present study is an

initial geophysical attempt for the first time over this region and has contributed significantly in understanding the subsurface configuration of the region.

Acknowledgements

The authors gratefully acknowledge the financial support (File No. ECR/2015/000247) of Science and Engineering Research Board (SERB), Department of Science and Technology, Government of India, to carry out this work. They also like to thank the Editor and two anonymous reviewers, whose painstaking reviews have helped to improve the overall quality of the manuscript.

References

Balaram V, Singh S P, Satyanarayanan M and Anjaiah K V 2013 Platinum group elements geochemistry of ultramafic and associated rocks from Pindar in Madawara igneous complex, Bundelkhand massif, central India; *J. Earth Syst. Sci.* **122(1)** 79–91, https://doi.org/10.1007/s12040-012-0260-0.

Baranov V 1957 A new method for interpretation of aeromagnetic anomalies: Pseudogravimetric anomalies; *Geophysics* **22** 359–383, https://doi.org/10.1190/1.1438369.

Basu A K 1986 Geology of parts of the Bundelkhand granite massif, central India; *Rec. Geol. Surv. India* **117** 61–124.

Basu A K 2007 Role of the Bundelkhand Granite Massif and the Son–Narmada megafault in precambrian crustal evolution and tectonism in central and western India; *J. Geol. Soc. India* **70** 745–770.

Bhattacharya A R and Singh S P 2013 Proterozoic crustal scale shearing in the Bundelkhand massif with special reference to quartz reefs; *J. Geol. Soc. India* **82** 474–484, https://doi.org/10.1007/s12594-013-0178-4.

Bhowmik S K, Wilde S A, Bhandari A, Pal T and Pant N C 2012 Growth of the Greater Indian Landmass and its assembly in Rodinia: Geochronological evidence from the Central Indian Tectonic Zone; *Gondwana Res.* **22** 54–72, https://doi.org/10.1016/j.gr.2011.09.008.

Blakely R J 1995 *Potential theory in gravity and magnetic applications*; Cambridge University Press, Cambridge, 464p.

Cai K, Sun M, Yuan C, Zhao G, Xiao W and Long X 2012 Keketuohai mafic–ultramafic complex in the Chinese Altai, NW China: Petrogenesis and geodynamic significance; *Chem. Geol.* **294–295** 26–41, https://doi.org/10.1016/j.chemgeo.2011.11.031.

Clark D A 1997 Magnetic petrophysics and magnetic petrology: Aids to geological interpretation of magnetic surveys; *AGSO J. Aust. Geol. Geophys.* **17** 83–103.

Ernst R E 2007 Mafic–ultramafic large igneous provinces (LIPs): Importance of the pre-Mesozoic record; *Episodes* **30** 108–114.

Farooqui S A and Singh A K 2006 Platinum mineralization in Ikauna Area, Lalitpur District, Uttar Pradesh; *J. Geol. Soc. India* **68(4)** 582–584.

Farooqui S A and Singh P K 2010 PGE mineralisation in ultramafic/mafic enclaves of Ikauna area Bundelkhand craton, India; In: *Adv. Geosci. Solid Earth* (ed.) Satake K, World Scientific Publishing Company **20** 111–120, https://doi.org/10.1142/9789812838186_0005.

Ma J, Lü X, Liu Y, Cao X, Liu Y, Ruan B and Adam M M A 2016 The impact of early sulfur saturation and calc-crustal contamination on ore-forming process in the Posan mafic–ultramafic complex: Derived from the shallow depleted mantle, Beishan region, NW China; *J. Asian Earth Sci.* **118** 81–94, https://doi.org/10.1016/j.jseaes.2015.12.020.

Meert J G and Pandit M K 2015 The Archaean and Proterozoic history of peninsular India: Tectonic framework for Precambrian sedimentary basins in India; *Geol. Soc. Lond. Memoir* **43** 29–54, https://doi.org/10.1144/M43.3.

Mohanty N, Singh S P, Satyanarayanan M, Jayananda M, Korakoppa M M and Hiloidari S 2018 Chromian spinel compositions from Madawara ultramafics, Bundelkhand Craton: Implications on petrogenesis and tectonic evolution of the southern part of Bundelkhand Craton, central India; *Geol. J.* **54** 2099–2123, https://doi.org/10.1002/gj.3286.

Mondal M E A, Goswami J N, Deomurari M P and Sharma K K 2002 Ion microprobe $^{207}Pb/^{206}Pb$ ages of zircons from the Bundelkhand massif, northern India: Implications for crustal evolution of the Bundelkhand–Aravalli protocontinent; *Precamb. Res.* **117** 85–100, https://doi.org/10.1016/S0301-9268(02)00078-5.

Nabighian M N 1972 The analytic signal of two-dimensional magnetic bodies with polygonal cross-section: Its properties and use for automated anomaly interpretation; *Geophysics* **37** 507–517, https://doi.org/10.1190/1.1440276.

Naganjaneyulu K and Santosh M 2010 The Central India Tectonic Zone: A geophysical perspective on continental amalgamation along a Mesoproterozoic suture; *Gondwana Res.* **18** 547–564, https://doi.org/10.1016/j.gr.2010.02.017.

Naidu P S 1970 Statistical structure of aeromagnetic field; *Geophysics* **35** 279–292, https://doi.org/10.1190/1.1440091.

Pacino M C and Introcaso A 1987 Regional anomaly determination using the upwards continuation method; *B. Geofis. Teor. Appl.* **29** 113–122.

Pati J K, Patel S C, Pruseth K L, Malviya V P, Arima M, Raju S and Prakash K 2007 Geology and geochemistry of giant quartz veins from Bundelkhand Craton, central India and their implications; *J. Earth Syst. Sci.* **116(6)** 497–510, https://doi.org/10.1007/s12040-007-0046-y.

Polat A, Appel P W U and Fryer B J 2011 An overview of the geochemistry of Eoarchean to Mesoarchean ultramafic to mafic volcanic rocks, SW Greenland: Implications for mantle depletion and petrogenetic processes at subduction zones in the early Earth; *Gondwana Res.* **20** 255–283, https://doi.org/10.1016/J.GR.2011.01.007.

Prakash R, Swarup P and Srivastava R N 1975 Geology and mineralization in the southern parts of Bundelkhand in Lalitpur district, Uttar Pradesh; *J. Geol. Soc. India* **16** 143–156.

Ramiz M M, Mondal M E A and Farooq S H 2018 Geochemistry of ultramafic–mafic rocks of the Madawara

Ultramafic Complex in the southern part of the Bundelkhand Craton, Central Indian Shield: Implications for mantle sources and geodynamic setting; *Geol. J.* **54** 2185–2207, https://doi.org/10.1002/gj.3290.

Ram Mohan M, Singh S P, Santosh M, Siddiqui M A and Balaram V 2012 TTG suite from the Bundelkhand Craton, central India: Geochemistry, petrogenesis and implications for Archean crustal evolution; *J. Asian Earth Sci.* **58** 38–50, https://doi.org/10.1016/j.jseaes.2012.07.006.

Reid A B, Allsop J M, Granser H, Millett A J and Somerton I W 1990 Magnetic interpretation in three dimensions using Euler deconvolution; *Geophysics* **55** 80–91, https://doi.org/10.1190/1.1442774.

Reid A B and Thurston J B 2014 The structural index in gravity and magnetic interpretation: Errors, uses, and abuses; *Geophysics* **79** J61–J66, https://doi.org/10.1190/geo2013-0235.1.

Roest W R and Pilkington M 1993 Identifying remanent magnetization effect in magnetic data; *Geophysics* **58** 653–659, https://doi.org/10.1190/1.1443449.

Roy A and Aina A O 1986 Some new magnetic transformations; *Geophys. Prospect.* **34** 1219–1232, https://doi.org/10.1111/j.13652478.1986.tb00525.x.

Satyanarayanan M, Balaram V, Roy P, Anjaiah V and Singh S P 2010 Trace, Rare Earth Element (REE) and Platinum Group Element (PGE) geochemistry of the mafic and ultramafic rocks from Bundelkhand craton, central India; In: *Adv. Geosci. Solid Earth* (ed.) Satake K, World Scientific Publishing Company **20** 57–79, https://doi.org/10.1142/9789812838186_0003.

Satyanarayanan M, Singh S P, Balaram V and Niranjan M 2015 Geochemistry of the Madawara Igneous Complex, Bundelkhand craton, Central India: Implications for PGE metallogeny; *Open Geosci.* **7** 836–853, https://doi.org/10.1515/geo-2015-0016.

Silva J B C 1986 Reduction to the pole as an inverse problem and its application to low-latitude anomalies; *Geophysics* **51** 369–382, https://doi.org/10.1190/1.1442096.

Singh S P, Balaram V, Satyanarayanan M, Anjaiah K V and Kharya A 2010a Madawara Ultramafics Complex in Bundelkhand Craton: A new PGE repository for exploration in central India; *J. Econ. Geol. Georesour. Manag.* **7** 51–68.

Singh S P, Balaram V, Satyanarayanan M, Anjaiah K V and Kharia A 2010b Platinum group elements in basic and ultrabasic rocks around Madawara, Bundelkhand Massif, central India; *Curr. Sci.* **99** 375–383.

Singh S P, Balaram V, Satyanarayanan M, Sarma D S, Subramanyam K S V, Anjaiah K V and Kharia A 2011 Platinum group minerals from the Madawara ultramafic–mafic complex, Bundelkhand massif, Central India: A preliminary note; *J. Geol. Soc. India* **78** 281–283.

Spector A and Grant F S 1970 Statistical methods for interpreting aeromagnetic data; *Geophysics* **35** 293–302, https://doi.org/10.1190/1.1440092.

Srivastava R, Basantaray A K and Mandal A 2018 Improved compact inversion approach for 2D gravity data modelling using probabilistic bounds; In: *80th EAGE Conference & Exhibition*, https://doi.org/10.3997/2214-4609.201801464.

Su B X, Qin K Z, Sakyi P A, Li X H, Yang Y H, Sun H, Tang D M, Liu P P, Xiao Q H and Malaviarachchi S P K 2011 U–Pb ages and Hf–O isotopes of zircons from Late Paleozoic mafic–ultramafic units in the southern Central Asian Orogenic Belt: Tectonic implications and evidence for an Early-Permian mantle plume; *Gondwana Res.* **20** 516–531, https://doi.org/10.1016/J.GR.2010.11.015.

Telford W M, Geldart L P and Sheriff R E 1990 *Applied geophysics*; Cambridge University Press, Cambridge, 771p.

Thompson D T 1982 EULDPH: A new technique for making computer-assisted depth estimates from magnetic data; *Geophysics* **47** 31–37, https://doi.org/10.1190/1.1441278.

Toft P B, Arkani-Hamed J and Haggerty S E 1990 The effects of serpentinization on density and magnetic susceptibility: A petrophysical model; *Phys. Earth Planet. Inter.* **65** 137–157, https://doi.org/10.1016/0031-9201(90)90082-9.

Tselentis G A, Drakopoulos J and Dimtriads K 1988 A spectral approach to Moho depths estimation from gravity measurement in Epirus (NW Greece); *J. Phys. Earth* **36** 255–266, https://doi.org/10.4294/jpe1952.36.255.

Yellappa T, Venkatasivappa V, Koizumi T, Chetty T R K, Santosh M and Tsunogae T 2014 The mafic–ultramafic complex of Aniyapuram, Cauvery Suture Zone, southern India: Petrological and geochemical constraints for Neoarchean suprasubduction zone tectonics; *J. Asian Earth Sci.* **95** 81–98, https://doi.org/10.1016/J.JSEAES.2014.04.023.

Corresponding editor: N V Chalapathi Rao